Accepted Manuscript

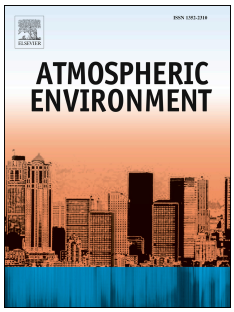

Characterization of Submicron Aerosols at a Suburban Site in Central China

Qingqing Wang, Jian Zhao, Wei Du, Godson Ana, Zhenzhu Wang, Lu Sun, Yuying Wang, Fang Zhang, Zhanqing Li, Xingnan Ye, Yele Sun

PII: S1352-2310(16)30088-7

DOI: 10.1016/j.atmosenv.2016.01.054

Reference: AEA 14434

To appear in: *Atmospheric Environment*

Received Date: 5 October 2015

Revised Date: 28 January 2016

Accepted Date: 29 January 2016

Please cite this article as: Wang, Q., Zhao, J., Du, W., Ana, G., Wang, Z., Sun, L., Wang, Y., Zhang, F., Li, Z., Ye, X., Sun, Y., Characterization of Submicron Aerosols at a Suburban Site in Central China, *Atmospheric Environment* (2016), doi: 10.1016/j.atmosenv.2016.01.054.

Characterization of Submicron Aerosols at a Suburban Site in Central China

Qingqing Wang[1,2], Jian Zhao[1], Wei Du[1], Godson Ana[3], Zhenzhu Wang[4], Lu Sun[4,2], Yuying Wang[5], Fang Zhang[5], Zhanqing Li[5], Xingnan Ye[6], Yele Sun[1,*]

[1]State Key Laboratory of Atmospheric Boundary Layer Physics and Atmospheric Chemistry, Institute of Atmospheric Physics, Chinese Academy of Sciences, Beijing 100029, China

[2]University of Chinese Academy of Sciences, Beijing 100049, China

[3]Department of Environmental Health Sciences, Faculty of Public Health, University of Ibadan, Ibadan, Nigeria

[4]Key Laboratory of Atmospheric Composition and Optical Radiation, Anhui Institute of Optics and Fine Mechanics, Chinese Academy of Sciences, Hefei 230031, China

[5]College of Global Change and Earth System Science, Beijing Normal University, Beijing 100875, China

[6]Department of Environmental Science & Engineering, Fudan University, Shanghai 200433, China

*Correspondence to: sunyele@mail.iap.ac.cn

Abstract

We have characterized the chemical composition and sources of submicron aerosol (PM_1) at a suburban site in Xinzhou in central China using an Aerosol Chemical Speciation Monitor from July 17 to September 5, 2014. The average (±1σ) PM_1 concentration was 35.4 (±20.8) μg/m^3 for the entire study period, indicating that Xinzhou was less polluted compared to the megacities in the North China Plain (NCP). The PM_1 was mainly composed of organic aerosol and sulfate, on average accounting for 33.1% and 32.4%, respectively, followed by nitrate (14.4%) and ammonium (11.8%). Higher sulfate and lower nitrate contributions than those in megacities in the NCP elucidated an important emission source of coal combustion in central China. Three organic aerosol (OA) factors, i.e., hydrocarbon-like OA (HOA), semi-volatile oxygenated OA (SV-OOA) and low-volatility OOA (LV-OOA), were identified using positive matrix factorization. Secondary OA (= SV-OOA + LV-OOA) dominated OA, on average accounting for 82%, indicating that OA at the Xinzhou site was overall oxidized. We also observed relatively similar aerosol bulk composition and OA composition at low and high mass loading periods, and also from the different source areas, indicating that aerosol species were homogeneously distributed over a regional scale near the site for most of the time during this study. Slightly higher mass concentrations and sulfate contributions from the southern air masses were likely due to the transport from the polluted cities, such as Taiyuan to the south. In addition, the daily variation of PM_1 in Xinzhou resembled that observed in Beijing, indicating that the wide-scale regional haze pollution often influences both the NCP and the central China.

Key Words:

Submicron aerosol; Organic aerosol; Composition; Sources; Central China

1. Introduction

Atmospheric pollution caused by high concentrations of aerosol particles is a major environmental problem in China (Chan and Yao, 2008; Yuan et al., 2015; Zhang et al., 2012). In addition to the direct and indirect climate effects by scattering and absorbing sunlight or serving as cloud condensation nuclei (CCN) (Stocker et al., 2013), aerosol also causes potential health risks and visibility problems (Chen et al., 2013).

In recent years, air pollution studies were extensively carried out in megacities in east China, such as Beijing (Guo et al., 2014; Sun et al., 2014; Sun et al., 2015), Shanghai (Cheng et al., 2015), Nanjing (Zhuang et al., 2014) and Guangzhou (Cui et al., 2015; Huang et al., 2011), including chemical compositions, optical properties, source apportionment, and meteorological effects. However, aerosol chemistry in the cities of central China has not been sufficiently investigated or given adequate attention (Yang et al., 2013). Therefore, our knowledge of the composition and sources of atmospheric aerosol in central China remains poor. In this study, we conducted a field campaign in Xinzhou, a city located to the west of Mountain Taihang (average elevation: 1500 m a.s.l.). Xinzhou is also located in Shanxi Basin, one of the largest coal bases in China (Zhong et al., 2014), which is approximately 80 km north of Taiyuan city. Some recent studies characterized aerosol particles in Taiyuan, and the results showed that coal combustion, vehicle exhaust and industrial emissions were the three major sources of fine particles (He et al., 2015; Li et al., 2014). However, few studies have been conducted in the northern area in central China. Shi et al. (2014a; 2014b) reported the levels, temporal and spatial distributions of carbonaceous aerosol and water-soluble ions during heating and non-heating periods in Xinzhou. Their results showed that coal combustion was a dominant source of organic carbon (OC) and elemental carbon (EC) during the heating period. The mass ratio of NO_3^-/SO_4^{2-} also indicated a dominant contribution of stationary sources, e.g., coal combustion, with a considerable contribution from vehicle emissions. However, most previous studies were based on filter measurements with the sampling duration in days and even weeks, our knowledge of the air pollution levels, daily variations, and meteorological effects in central China remains less understood.

Here an Aerodyne Aerosol Chemical Speciation Monitor (ACSM) was deployed for the first time at a suburban site in Xinzhou in central China (Fig. 1), from July 17 to September 5, 2014 as an integral part of the Atmosphere, Aerosol, Cloud, and CCN (A^2C^2) campaign (Zhang et al., 2015). A major goal of this campaign was to investigate the relationship between aerosol composition and hygroscopicity and CCN. In this work, we have a detailed characterization of submicron aerosol composition, diurnal variations, and the influences of meteorological variables on aerosol characteristics. Also, the composition and sources of organic aerosol (OA) are investigated using positive matrix factorization (PMF) analysis, and the major source areas of aerosol particles are discussed.

2. Materials and methods

2.1. Sampling site

The sampling site is located at Xinfuqu National Meteorological Observatory (38.07°N, 112.12°E) (700 m a.s.l.), which is a suburban site in Xinzhou in Xinding Basin. The site was surrounded by agricultural crops land with minor influences from industry emissions. A national road G108 is located at approximately 100 m to the east. The meteorological conditions during the study period are presented in Fig. 2. Wind speed was generally below 4 m/s with the prevailing winds from the north and the west (Fig. S1). The average temperature and relative humidity (RH) was 21.4 ^{o}C and 70 %, respectively, for the entire study period.

2.2. Measurements

All instruments were placed in an air-conditioned container with the sampling heights being approximately 5 m. Non-refractory PM_1 (NR-PM_1) species including organic aerosol (Org), sulfate (SO_4^{2-}), nitrate (NO_3^-), ammonium (NH_4^+) and chloride (Cl^-) were measured by the ACSM at a time resolution of ~8 min (Ng et al., 2011). The aerosol sampling set-up and the ACSM operations in this study were overall similar to those employed in previous studies in Beijing (Sun et al., 2012a). Briefly, the ambient air was drawn inside the container through a 1/2 inch (outer diameter) stainless steel tube using an external pump (~3 L/min), of which ~0.1 L/min was isokinetically sub-sampled into the ACSM. A $PM_{2.5}$ cyclone (Model:

URG-2000-30ED) was placed in front of the sampling inlet to remove coarse particles larger than 2.5 μm. Aerosol particles were dried using a silica gel diffusion dryer before entering the ACSM. A more detailed operation of the ACSM was given in Sun et al. (2012a).

Black carbon (BC) in $PM_{2.5}$ was measured by a 7-wavelength Aethalometer (Model AE31, Magee Scientific Corp.) at a time resolution of 5 min. In addition, a Scanning Mobility Particle Sizer (SMPS, TSI, Model 3034) equipped with a long Differential Mobility Analyzer (DMA) was simultaneously operated to measure the size-resolved particle number concentrations between 11 – 594 nm at a time resolution of 5 min. Gaseous species of O_3 (Model 49i), NO/NO_2 (Model 42i), and SO_2 (Model 43i) were also measured by a range of gas analyzers from Thermo Scientific. The hourly-average meteorological data including wind speed (WS), wind direction (WD), temperature (*T*), pressure (*P*), RH and precipitation (Precip.) were obtained from the Meteorological Observatory at the site.

2.3. ACSM data analysis

The mass concentration and chemical composition of NR-PM_1 species were analyzed with the ACSM standard data analysis software (v 1.5.3.0, https://sites.google.com/site/ariacsm/mytemplate-sw) within Igor Pro (Wave Metrics, Inc., Oregon, USA). A collection efficiency (CE) of 0.5 was applied to account for the incomplete detection of particles primarily due to the particle bounce effect (Matthew et al., 2008). It has been found that CE can be composition-dependent, particularly sensitive to the fraction of ammonium nitrate, and also influenced by RH and particle acidity (Middlebrook et al., 2012). In this study, sulfate dominated the NR-PM_1 mass, with a small amount of ammonium nitrate (18.5% of PM_1 on average). Also, aerosol particles were slightly acidic as suggested by the average ratio (0.68) of measured NH_4^+ to the predicted NH_4^+ (= $SO_4^{2-}/96\times18\times2$ + $NO_3^-/62\times18$ + $Cl^-/35.5\times18$) that is required to fully neutralize SO_4^{2-}, NO_3^-, and Cl^- (Zhang et al., 2007b). These results together suggest that the ammonium nitrate fraction, RH and particle acidity could not affect CE substantially. In addition, the number concentrations measured by the SMPS were converted to the mass concentrations using chemically-resolved particle density that was estimated from the chemical

137 composition of PM_1 (Salcedo et al., 2006). The PM_1 (= NR-PM_1 + BC) tracks well
138 with that of SMPS (r^2 = 0.65), and the mass ratio of SMPS to ACSM is 0.62 (Fig. S2),
139 likely due to the limited size range of SMPS measurements by missing a considerable
140 fraction of particles between 590 – 1000 nm. Overall, a CE of 0.5 was found to be
141 appropriate for this site.

142 The ACSM organic mass spectra were analyzed by PMF to resolve potential OA
143 components with different sources and processes. The PMF analysis with the
144 algorithm PMF2.exe (Paatero and Tapper, 1994) was performed on the OA mass
145 spectra matrix between *m/z* 12 and 125. The *m/z*'s above 125 with interferences from
146 naphthalene signals and larger uncertainties due to the ion transmission efficiencies
147 were excluded from the PMF analysis. The PMF results were then evaluated using the
148 PMF Evaluation Tool (PET, v 2.06) (Ulbrich et al., 2009) following the procedures
149 given by Zhang et al. (2011). After a careful evaluation of the mass spectral profiles,
150 diurnal variations, and also comparisons of OA factors with other external species
151 (Table S1), a three factor solution with rotational forcing parameter (FPEAK) = 0.6
152 was selected. The three OA factors are hydrocarbon-like OA (HOA), semi-volatile
153 oxygenated OA (SV-OOA), and low-volatility OOA (LV-OOA). More detailed PMF
154 diagnostic are presented in Figs. S3 and S4.

155 *2.4. Backward trajectory analysis*

156 The 72 h backward trajectories at a height of 500 m were calculated every hour
157 using the Hybrid Single-Particle Lagrangian Integrated Trajectory (HYSPLIT,
158 version 4.8) model (Draxler and Rolph, 2013) for the sampling period. The back
159 trajectories were then grouped into 5 clusters using the cluster analysis algorithm,
160 which were from the south (Cluster 1, 13% of the time), the east (Cluster 2, 28%), the
161 west (Cluster 3, 26%), the north (Cluster 4, 16%), and the northwest (Cluster 5, 17%).

162 **3. Results and discussion**

163 *3.1. Mass concentrations*

164 Fig. 2 shows the time series of meteorological parameters and submicron aerosol
165 composition. The average (±1σ) PM_1 concentration during the entire study period was
166 35.4 (±20.8) μg/m^3, with daily average concentration ranging from 12.0 to 72.3 μg/m^3.

Considering that PM_1 generally contributed ~60 – 70% of $PM_{2.5}$ in China (Wang et al., 2015b), the mass concentration of $PM_{2.5}$ derived from the PM_1 mass in Xinzhou city was generally below the secondary class of National Ambient Air Quality Standards (NAAQS, 75 μg/m^3 for a 24 hour average), and also lower than those reported in megacities in North China Plain (Sun et al., 2015; Zhao et al., 2013), indicating a lighter PM pollution during this study period. Organic aerosol and sulfate comprised the major fraction of PM_1, on average accounting for 33.1% and 32.4%, respectively, followed by nitrate (14.4%), ammonium (11.8%), black carbon (6.9%), and chloride (1.5%). Compared to those observed in summer in the megacity of Beijing (Sun et al., 2012a), the aerosol composition in Xinzhou showed substantially higher contribution of sulfate (32.4% vs. 18%) and correspondingly lower nitrate (14.4% vs. 25%). These results suggest dominant stationary sources, e.g., coal combustion emissions, over mobile sources in this region. Indeed, the average concentration of sulfate (11.5 μg/m^3) was even higher than that (9.0 μg/m^3) observed in summer in Beijing, whereas the nitrate concentration was much lower (5.1 vs. 12.4 μg/m^3).

3.2. Identification of OA factors with PMF

PMF analysis of ACSM OA mass spectra resolved three OA factors with different sources and processes. The mass spectra and time series of the three OA factors are shown in Fig. 3. The average mass concentrations of HOA, SV-OOA, LV-OOA were 2.2, 4.3, 5.2 μg/m^3, respectively for the entire study (Fig. 4a). The two secondary OA (SOA) factors were both characterized by the prominent peak of *m/z* 44 (mainly CO_2^+) (Aiken et al., 2009). The f_{44} (fraction of *m/z* 44 in OA) for SV-OOA and LV-OOA was 0.22 and 0.29, respectively. Higher *f*44 in LV-OOA indicated the more oxidized properties of LV-OOA than SV-OOA (Aiken et al., 2008). This is consistent with the results from previous studies that LV-OOA and SV-OOA are used as a surrogate of more oxidized and less oxidized SOA, respectively (Jimenez et al., 2009). Indeed, LV-OOA was highly correlated with the non-volatile sulfate (r = 0.90) whereas SV-OOA correlated better with semi-volatile ammonium (r = 0.63) (Table S1). LV-OOA showed a pronounced diurnal cycle with higher concentration during daytime and lower concentration at night (Fig. 5e). Such a diurnal variation was similar to those of temperature and O_3, indicating a daytime photochemical

production. Whereas, the diurnal cycle of SV-OOA showed some similarities to those of HOA and NO_x. One explanation is that part of SV-OOA was likely produced from the oxidation of primary organic aerosol (r = 0.93, Table S1).

The mass spectral pattern of HOA was characterized by hydrocarbon ion series, $C_nH_{2n-1}^+$ and $C_nH_{2n+1}^+$, which is similar to that of diesel exhausts (Canagaratna et al., 2004) and those of HOA resolved at various urban sites (Aiken et al., 2009; He et al., 2011; Sun et al., 2012a). It should be noted that the HOA factor cannot be separated from cooking OA (COA) in summer in Beijing by PMF analysis of unit mass resolution spectra (Sun et al., 2010; Sun et al., 2012a), as a result, the HOA spectrum often showed high *m/z* 55/57 ratio due to the influences of cooking aerosol (Mohr et al., 2012). In contrast, the HOA spectrum in this study showed comparable *m/z* 55 and *m/z* 57 (*m/z* 55/57 = 1.3), which is much lower than the typical value of *m/z* 55/57 in COA (~2.5) (Sun et al., 2013; Xu et al., 2015), indicating that cooking emission was not likely an important contributor to this factor. We further checked the diurnal cycle of the residual of *m/z* 55 (Fig. S5) and didn't observe clear peaks at meal times, further supporting the insignificant cooking sources in this study. This is consistent with the fact that the sampling site is far away from the city center and less affected by the cooking emissions. In addition, *f*60 (fraction of *m/z* 60 in OA) was relatively constant throughout the study with an average value closed to 0.3% (Fig. S6) in the absence of biomass burning (Cubison et al., 2011). This result indicated that there were no significant biomass burning emissions during the study period. Although previous studies showed that coal combustion was an important contribution of PM in Xinzhou (Shi et al., 2014a; Shi et al., 2014b), we didn't resolve a primary CCOA factor in this study, likely due to (1) the similar mass spectrum of CCOA and HOA (Sun et al., 2013) and the low sensitivities of the ACSM measurements, thus HOA in Xinzhou was posssibly mixed with CCOA, and (2) the measurements were conducted in a suburban area with much less coal combustion emissions compared to the city of Taiyuan, thus CCOA in Xinzhou was likely mainly from regional transport. HOA correlated well with BC - a tracer for combustion emissions (r = 0.75) (Aiken et al., 2009). The average ratio of HOA/BC (0.93) was (Wang et al., 2015a) lower than that observed in high polluted periods in Beijing (1.5) (Sun et al., 2014; Wang et al.,

2015a), yet similar to that observed in New York City (Sun et al., 2011; Sun et al., 2012b) and Mexico City (Aiken et al., 2009).*3.3. Submicron aerosol composition and diurnal variations*

Fig. 4 presents the average submicron aerosol composition and OA composition for the entire study, and also the periods with low (< 35 μg/m^3) and high aerosol mass loadings (≥ 35 μg/m^3) with statistics of all data points. Secondary organic aerosol (= SV-OOA + LV-OOA) dominated OA, on average accounting for 82% with the rest being primary OA (POA). The contribution of SOA was overall higher than that (~60%) observed in summer in megacities in North China Plain (Sun et al., 2014), yet close to those observed at rural/remote sites (Zhang et al., 2007a) . These results suggest that OA at the suburban site in Xinzhou was relatively well oxidized. Aerosol composition showed some differences between low and high mass loading periods (Fig. 4). Secondary inorganic aerosol (SIA) including sulfate, nitrate, and ammonium showed enhanced contributions to PM_1 during high mass loading periods, while that of organic aerosol showed a corresponding decrease. For example, the contribution of SIA was increased by 8.2% from 53.2% during low mass loading periods to 61.4% during high mass loading periods, while BC and organic aerosol were decreased by 1.7% and 5.8%, respectively. It is interesting to note that OA composition was rather similar between low and high mass loading periods, which were both dominated by SOA (82 – 83%). These results might suggest the similar aging processes of OA across different mass loadings, particularly in the relatively isolated basin in central China.

The diurnal profile of sulfate (Fig. 5) was relatively flat, consistent with its regional characteristics. However, a visible increase was observed between 6:00 – 15:00 when wind direction showed a change from the north to the south. Considering that the gas precursor of SO_2 showed a large increase between 6:00 – 10:00, and maintained at a relatively high level until 18:00, regional transport from the south rather than photochemical transformation might play the dominant role in driving the diurnal variation of sulfate. This is further supported by the higher sulfate concentration from the east and the south than other wind directions (Figs. 6a and 7a). The diurnal profile of nitrate was quite different from that of sulfate. As shown in Fig.

5c, nitrate showed a pronounced diurnal cycle with higher concentration at nighttime and lower values during daytime. Such a diurnal cycle driven by the temperature dependent gas-particle partitioning of NH_4NO_3 and planetary boundary layer (PBL) has been observed many times in megacities (Ianniello et al., 2011; Sun et al., 2012a; Xu et al., 2014). Indeed, while organic aerosol and sulfate present increases as the increase of *T* at >25°C (Fig. 6a), the nitrate concentration showed a rapid decrease instead, indicating the evaporative loss of ammonium nitrate by partitioning to gaseous HNO_3 and NH_3. Consistently, semi-volatile ammonium chloride showed remarkably similar diurnal variations and *T* dependence as ammonium nitrate. Note that the diurnal peak concentration of nitrate was approximately 1 hour behind chloride indicating the photochemical production of nitrate particles in early morning also played a role. We also observed a strong RH dependence of nitrate. As RH increased from 20% to more than 80%, the nitrate concentration showed a rapid increase from less than 2 $\mu g/m^3$ to 7 $\mu g/m^3$, and correspondingly, the nitrate contribution to PM_1 increased from less than 10% to ~20% (Figs. 6a and b). This result might suggest that nitrate played an enhanced role in PM pollution at high RH levels, which was most likely due to the transformation of gaseous HNO_3 into liquid-phase particles.

The diurnal cycles varied differently between different OA factors. HOA showed a pronounced diurnal cycle with two peaks occurring in the morning and evening rush hours. The diurnal cycle of HOA was similar to those of NO_x and BC, indicating the dominant traffic sources for these three species. Note that the low concentrations during the late afternoon were likely due to the elevated PBL. Interestingly, the diurnal profile of SV-OOA showed some similarities to that of HOA, implying that a considerable fraction of SV-OOA might share the same sources as HOA, e.g., from the oxidation of HOA. The diurnal cycle of LV-OOA presented a noon peak associated with high mixing ratio of O_3, indicating clear daytime photochemical production. However, the variation of LV-OOA concentration was relatively flat in the rest of the day, illustrating the regional characteristic of LV-OOA. Thus, such a diurnal variation of LV-OOA was likely from a combined result of photochemical production and regional transport. LV-OOA dominated OA throughout the day (~40

– 50%), highlighting the dominance of aged OA at the suburban site in central China.

We further investigated the variations of aerosol species as a function of meteorological variables (Fig. 6). All aerosol species showed decreased concentrations with the increase in wind speed, indicating a diluting effect of winds on PM pollution. However, the diluting rates by winds were much lower compared to those observed in wintertime in Beijing (Sun et al., 2013). These results might suggest that aerosol particles were relatively homogeneously distributed in this area, as a result, the winds showed a smaller impact in diluting aerosol species than that in megacity of Beijing. Indeed, aerosol mass concentrations and chemical composition were relatively similar across different wind directions except higher organic aerosol and sulfate from the east to the south due to the transport from the polluted areas to the south (Fig. 6).

All PM_1 species increased significantly as a function of RH at low levels (< 45%), yet varied differently above 45%. While organic aerosol and sulfate presented the highest concentrations at RH = ~60%, nitrate and chloride increased continuously as the increase of RH, indicating a larger impact of RH on these two species. The reasons were likely due to the transformation of gaseous HNO_3 and HCl into liquid phase particles at high RH levels. Note that high RH levels generally occurred at nighttime when *T* was low. The low *T* also facilitated the gas-particle partitioning of ammonium nitrate and ammonium chloride particles. As shown in Fig. 6b, organic aerosol dominated PM_1 at low RH levels, while SIA showed an enhanced role at high RH levels. This illustrated a different role of organic aerosol and SIA in PM pollution between clean periods (low RH) and polluted events (high RH). The *T*-dependence was also different between different aerosol species. Organic aerosol and sulfate increased continuously as the increase of *T*. Such a *T*-dependence behavior indicated the photochemical production of these two species given that higher *T* was often associated with higher solar radiation and O_3. While nitrate and chloride showed increases as a function of *T* below 20°C, their concentrations were rapidly decreased at higher *T* due to the evaporative loss. The refractory BC appeared not to be *T*-dependent and showed minor variations across different *T*. As a result, aerosol composition varied substantially at low and high *T*. While organic aerosol and BC

were two dominant species of PM_1 at low *T*, the sulfate contribution was significantly elevated from 20% to more than 40% at $T > 30$°C.

3.4. Source areas of PM_1 species

Fig. 7 shows the average chemical composition of PM_1 for five clusters from different source areas. The air masses during the study period were dominantly from the east cluster (C2, 28% of the time) with an average PM loading of 43 µg/m^3. C2 originated from the east of Mountain Taihang where many highly polluted cities are located, e.g., Shijiazhuang with an average $PM_{2.5}$ of 145.7 µg/m^3 in summer in 2009 (Zhao et al., 2013). Sulfate contributed the largest fraction of PM_1, accounting for 36% followed by organic aerosol (30%) during C2. Another cluster (C1, 13% of the time) originating from the south was also characterized by high PM loading (48 µg/m^3) and high contribution of sulfate (39%). This is consistent with the trajectories of C1 that passed through a highly polluted city, Taiyuan, to the south (The average $PM_{2.5}$ concentration was 135.8 µg/m^3 in summer in 2009) (He et al., 2015). The high aerosol mass loadings for these two clusters indicated that the high PM pollution at the sampling site was mainly influenced by these two source regions, i.e., the east and the south (C2 and C1). This was also supported by the wind direction dependence of aerosol species (Fig. 6a) which showed higher concentrations of organic aerosol and sulfate from the east and the south. Two clusters (C4 and C5) originating from the north showed largely different aerosol chemistry. Considering that the average *T* and RH was rather similar for five clusters (Table S2), the compositional differences among different clusters were mainly attributed to different source areas. While C5 (17% of the time) showed the lowest mass loading (20 µg/m^3) among five clusters, the average PM loading for C4 (39 µg/m^3) was actually similar to the other three clusters. These results suggested that the cluster of C5 originating from Mongolia brought clean air masses with substantially different aerosol composition compared with other clusters. SIA showed a great decrease from 54 – 66% to 44%, whereas primary chemical species, e.g., BC and HOA showed corresponding increases, indicating an enhanced role of local emissions during C5. It is interesting to note that the aerosol bulk compositions of four clusters (C1 – C4) from different source areas were overall similar except higher sulfate contribution from the south, for example,

14 – 16% for LV-OOA, 13 – 15% for nitrate, and 30 – 39% for sulfate. Results here indicated a similar aerosol composition over a regional scale near the Xinzhou city. We further checked the variation of $PM_{2.5}$ observed during the same time in Beijing. As shown in Fig. 7b, the daily variation of PM in Xinzhou was overall similar to that in Beijing, indicating the regional haze pollution over both the north China plain and the central China. Indeed, the MODIS satellite images showed that regional haze pollution on the west and east of Mountain Taihang was often connected (Fig. S7).

4. Conclusion

The chemical composition and sources of submicron aerosol at a suburban site in Xinzhou city in central China was characterized. The average PM_1 concentration was 35.4 $\mu g/m^3$ during this study period, indicating that the Xinzhou city was less polluted compared with the megacities in North China Plain. The PM_1 was dominantly contributed by organic aerosol (33.1%) and sulfate (32.4%), followed by nitrate (14.4%) and ammonium (11.8%). Higher sulfate and lower nitrate contributions than those in megacities in eastern China likely indicated an important source of coal combustion emissions in central China. PMF analysis resolved three OA factors from different sources and processes. SOA dominated OA, on average accounting for 82%, indicating that OA was overall oxidized during this study period. Aerosol composition was similar at low and high mass loading periods with slightly higher contribution of SIA at high PM levels. The sources of aerosol particles were investigated using back trajectories analysis. Although relatively higher mass loadings and higher contribution of sulfate were observed from the southern and the eastern air masses, submicron aerosol composition and OA composition were overall similar between different clusters from different source areas. Our results illustrated that aerosol species in the Xinding Basin in central China was homogeneously distributed over a regional scale. Also, the daily variation of PM in Xinzhou was overall similar to that in Beijing, indicating the wide-scale regional haze pollution over both the north China plain and the central China.

Acknowledgments

This work was supported by the National Key Basic Research Program of China

(2013CB955801) and the Strategic Priority Research Program (B) of the Chinese Academy of Sciences (XDB05020501). We also thank the team members for their assistance during the A^2C^2 campaign.

References

Aiken, A., Salcedo, D., Cubison, M.J., Huffman, J., DeCarlo, P., Ulbrich, I.M., Docherty, K.S., Sueper, D., Kimmel, J., Worsnop, D.R., 2009. Mexico City aerosol analysis during MILAGRO using high resolution aerosol mass spectrometry at the urban supersite (T0)–Part 1: Fine particle composition and organic source apportionment. Atmospheric Chemistry and Physics 9, 6633-6653.

Aiken, A.C., Decarlo, P.F., Kroll, J.H., Worsnop, D.R., Huffman, J.A., Docherty, K.S., Ulbrich, I.M., Mohr, C., Kimmel, J.R., Sueper, D., Sun, Y., Zhang, Q., Trimborn, A., Northway, M., Ziemann, P.J., Canagaratna, M.R., Onasch, T.B., Alfarra, M.R., Prevot, A.S.H., Dommen, J., Duplissy, J., Metzger, A., Baltensperger, U., Jimenez, J.L., 2008. O/C and OM/OC ratios of primary, secondary, and ambient organic aerosols with high-resolution time-of-flight aerosol mass spectrometry. Environmental science & technology 42, 4478-4485.

Canagaratna, M.R., Jayne, J.T., Ghertner, D.A., Herndon, S., Shi, Q., Jimenez, J.L., Silva, P.J., Williams, P., Lanni, T., Drewnick, F., 2004. Chase studies of particulate emissions from in-use New York City vehicles. Aerosol Science and Technology 38, 555-573.

Chan, C.K., Yao, X., 2008. Air pollution in mega cities in China. Atmospheric Environment 42, 1-42.

Chen, R.J., Zhao, Z.H., Kan, H.D., 2013. Heavy Smog and Hospital Visits in Beijing, China. American Journal of Respiratory and Critical Care Medicine 188, 1170-1171.

Cheng, Z., Jiang, J.K., Chen, C.H., Gao, J., Wang, S.X., Watson, J.G., Wang, H.L., Deng, J.G., Wang, B.Y., Zhou, M., Chow, J.C., Pitchford, M.L., Hao, J.M., 2015. Estimation of Aerosol Mass Scattering Efficiencies under High Mass Loading: Case Study for the Megacity of Shanghai, China. Environmental Science & Technology 49, 831-838.

Cubison, M.J., Ortega, A.M., Hayes, P.L., Farmer, D.K., Day, D., Lechner, M.J., Brune, W.H., Apel, E., Diskin, G.S., Fisher, J.A., Fuelberg, H.E., Hecobian, A., Knapp, D.J., Mikoviny, T., Riemer, D., Sachse, G.W., Sessions, W., Weber, R.J., Weinheimer, A.J., Wisthaler, A., Jimenez, J.L., 2011. Effects of aging on organic aerosol from open biomass burning smoke in aircraft and laboratory studies. Atmospheric Chemistry and Physics 11, 12049-12064.

Cui, H.Y., Chen, W.H., Dai, W., Liu, H., Wang, X.M., He, K.B., 2015. Source apportionment of $PM_{2.5}$ in Guangzhou combining observation data analysis and chemical transport model simulation. Atmospheric Environment 116, 262-271.

Draxler, R.R., Rolph, G.D., 2013. HYSPLIT (HYbrid Single-Particle Lagrangian Integrated Trajectory) Model access via NOAA ARL READY Website (http://www.arl.noaa.gov/HYSPLIT.php). NOAA Air Resources Laboratory, College Park, MD.

Guo, S., Hu, M., Zamora, M.L., Peng, J., Shang, D., Zheng, J., Du, Z., Wu, Z., Shao,

M., Zeng, L., Molina, M.J., Zhang, R., 2014. Elucidating severe urban haze formation in China. Proceedings of the National Academy of Sciences 111, 17373-17378.

He, L.Y., Huang, X.F., Xue, L., Hu, M., Lin, Y., Zheng, J., Zhang, R., Zhang, Y.H., 2011. Submicron aerosol analysis and organic source apportionment in an urban atmosphere in Pearl River Delta of China using high-resolution aerosol mass spectrometry. Journal of Geophysical Research 116, doi:10.1029/2010JD014566.

He, Q.S., Guo, W.D., Zhang, G.X., Yan, Y.L., Chen, L.G., 2015. Characteristics and Seasonal Variations of Carbonaceous Species in $PM_{2.5}$ in Taiyuan, China. Atmosphere 6, 850-862.

Huang, X. F., He, L. Y., Hu, M., Canagaratna, M., Kroll, J., Ng, N., Zhang, Y. H., Lin, Y., Xue, L., Sun, T. L., 2011. Characterization of submicron aerosols at a rural site in Pearl River Delta of China using an Aerodyne High-Resolution Aerosol Mass Spectrometer. Atmospheric Chemistry and Physics 11, 1865-1877.

Ianniello, A., Spataro, F., Esposito, G., Allegrini, I., Hu, M., Zhu, T., 2011. Chemical characteristics of inorganic ammonium salts in PM2.5 in the atmosphere of Beijing (China). Atmospheric Chemistry and Physics 11, 10803-10822.

Jimenez, J., Canagaratna, M., Donahue, N., Prevot, A., Zhang, Q., Kroll, J., DeCarlo, P., Allan, J., Coe, H., Ng, N., 2009. Evolution of organic aerosols in the atmosphere. Science 326, 1525-1529.

Li, R.J., Kou, X.J., Geng, H., Dong, C., Cai, Z.W., 2014. Pollution characteristics of ambient $PM_{2.5}$-bound PAHs and NPAHs in a typical winter time period in Taiyuan. Chinese Chemical Letters 25, 663-666.

Matthew, B.M., Middlebrook, A.M., Onasch, T.B., 2008. Collection efficiencies in an Aerodyne Aerosol Mass Spectrometer as a function of particle phase for laboratory generated aerosols. Aerosol Science and Technology 42, 884-898.

Middlebrook, A.M., Bahreini, R., Jimenez, J.L., Canagaratna, M.R., 2012. Evaluation of Composition-Dependent Collection Efficiencies for the Aerodyne Aerosol Mass Spectrometer using Field Data. Aerosol Science and Technology 46, 258-271.

Mohr, C., DeCarlo, P., Heringa, M., Chirico, R., Slowik, J., Richter, R., Reche, C., Alastuey, A., Querol, X., Seco, R., 2012. Identification and quantification of organic aerosol from cooking and other sources in Barcelona using aerosol mass spectrometer data. Atmospheric Chemistry and Physics 12, 1649-1665.

Ng, N.L., Herndon, S.C., Trimborn, A., Canagaratna, M.R., Croteau, P., Onasch, T.B., Sueper, D., Worsnop, D.R., Zhang, Q., Sun, Y., 2011. An Aerosol Chemical Speciation Monitor (ACSM) for routine monitoring of the composition and mass concentrations of ambient aerosol. Aerosol Science and Technology 45, 780-794.

Paatero, P., Tapper, U., 1994. Positive matrix factorization - A nonnegative factor model with optimal utilization of error estimates of data values. Environmetrics 5, 111-126.

Salcedo, D., Onasch, T.B., Dzepina, K., Canagaratna, M., Zhang, Q., Huffman, J., DeCarlo, P., Jayne, J., Mortimer, P., Worsnop, D.R., 2006. Characterization of ambient aerosols in Mexico City during the MCMA-2003 campaign with Aerosol Mass Spectrometry: results from the CENICA Supersite. Atmospheric Chemistry and Physics 6, 925-946.

Shi, M.X., Peng, L., Bai, H.L., Mu, L., Liu, F.X., Yang, H., 2014a. Characterization of water-soluble anions in PM_{10} and TSP in Xinzhou City. Acta Scientiae

Circumstantiae 34, 1825-1832.

Shi, M.X., Peng, L., Liu, X.F., Mu, L., Bai, H.L., Liu, F.X., Yang, H., 2014b. Characterization of organic and elemental carbon in PM_{10} in Xinzhou City. Environmental Science 35, 458-463.

Stocker, T., Qin, D., Plattner, G., Tignor, M., Allen, S., Boschung, J., Nauels, A., Xia, Y., Bex, V., Midgley, P., 2013. Summary for policymakers. Climate change 2013: the physical science basis. Contribution of Working Group I to the fifth assessment report of the Intergovernmental Panel on Climate Change. IPCC Localised 9, 2013.

Sun, J., Zhang, Q., Canagaratna, M.R., Zhang, Y., Ng, N.L., Sun, Y., Jayne, J.T., Zhang, X., Zhang, X., Worsnop, D.R., 2010. Highly time-and size-resolved characterization of submicron aerosol particles in Beijing using an Aerodyne Aerosol Mass Spectrometer. Atmospheric Environment 44, 131-140.

Sun, Y., Jiang, Q., Wang, Z., Fu, P., Li, J., Yang, T., Yin, Y., 2014. Investigation of the sources and evolution processes of severe haze pollution in Beijing in January 2013. Journal of Geophysical Research 119, 4380-4398.

Sun, Y., Wang, Z., Dong, H., Yang, T., Li, J., Pan, X., Chen, P., Jayne, J.T., 2012a. Characterization of summer organic and inorganic aerosols in Beijing, China with an Aerosol Chemical Speciation Monitor. Atmospheric Environment 51, 250-259.

Sun, Y., Wang, Z., Du, W., Zhang, Q., Wang, Q., Fu, P., Pan, X., Li, J., Jayne, J., Worsnop, D., 2015. Long-term real-time measurements of aerosol particle composition in Beijing, China: seasonal variations, meteorological effects, and source analysis. Atmospheric Chemistry and Physics 15, 14549-14591.

Sun, Y., Wang, Z., Fu, P., Yang, T., Jiang, Q., Dong, H., Li, J., Jia, J., 2013. Aerosol composition, sources and processes during wintertime in Beijing, China. Atmospheric Chemistry and Physics 13, 4577-4592.

Sun, Y.L., Zhang, Q., Schwab, J., Demerjian, K., Chen, W.N., Bae, M.S., Hung, H.M., Hogrefe, O., Frank, B., Rattigan, O., 2011. Characterization of the sources and processes of organic and inorganic aerosols in New York city with a high-resolution time-of-flight aerosol mass apectrometer. Atmospheric Chemistry and Physics 11, 1581-1602.

Sun, Y.L., Zhang, Q., Schwab, J.J., Chen, W.N., Bae, M.S., Hung, H.M., Lin, Y.C., Ng, N.L., Jayne, J., Massoli, P., 2012b. Characterization of near-highway submicron aerosols in New York City with a high-resolution aerosol mass spectrometer. Atmospheric Chemistry and Physics 12, 2215-2227.

Ulbrich, I., Canagaratna, M., Zhang, Q., Worsnop, D., Jimenez, J., 2009. Interpretation of organic components from Positive Matrix Factorization of aerosol mass spectrometric data. Atmospheric Chemistry and Physics 9, 2891-2918.

Wang, Q., Sun, Y., Jiang, Q., Du, W., Sun, C., Fu, P., Wang, Z., 2015a. Chemical composition of aerosol particles and light extinction apportionment before and during heating season in Beijing, China. Journal of Geophysical Research 120, 12708-12722.

Wang, Y.Q., Zhang, X.Y., Sun, J.Y., Zhang, X.C., Che, H.Z., Li, Y., 2015b. Spatial and temporal variations of the concentrations of PM10, PM2.5 and PM1 in China. Atmospheric Chemistry & Physics Discussions 15, 15319-15354.

Xu, J., Zhang, Q., Chen, M., Ge, X., Ren, J., Qin, D., 2014. Chemical composition,

sources, and processes of urban aerosols during summertime in Northwest China: insights from High Resolution Aerosol Mass Spectrometry. Atmospheric Chemistry & Physics 14, 16187-16242.

Xu, W.Q., Sun, Y.L., Chen, C., Du, W., Han, T.T., Wang, Q.Q., Fu, P.Q., Wang, Z.F., Zhao, X.J., Zhou, L.B., 2015. Aerosol composition, oxidative properties, and sources in Beijing: results from the 2014 Asia-Pacific Economic Cooperation Summit study. Atmospheric Chemistry & Physics 15, 13681-13698.

Yang, X., Yao, Z., Li, Z., Fan, T., 2013. Heavy air pollution suppresses summer thunderstorms in central China. Journal of Atmospheric and Solar-Terrestrial Physics s 95-96, 28-40.

Yuan, X.L., Mu, R.M., Zuo, J., Wang, Q.S., 2015. Economic Development, Energy Consumption, and Air Pollution: A Critical Assessment in China. Human and Ecological Risk Assessment 21, 781-798.

Zhang, F., Li, Z., Li, Y., Sun, Y., Wang, Z., Sun, L., Cribb, M., Zhao, C., Li, P., Wang, Q., 2015. Challenges of parameterizing CCN due to changes in particle physicochemical properties: implications from observations at a suburban site in China. Atmospheric Chemistry and Physics Discussions, 16141-16174.

Zhang, Q., He, K.B., Huo, H., 2012. Cleaning China's air. Nature 484, 161-162.

Zhang, Q., Jimenez, J.L., Canagaratna, M.R., Allan, J.D., Coe, H., Ulbrich, I., Alfarra, M.R., Takami, A., Middlebrook, A.M., Sun, Y.L., Dzepina, K., Dunlea, E., Docherty, K., DeCarlo, P.F., Salcedo, D., Onasch, T., Jayne, J.T., Miyoshi, T., Shimono, A., Hatakeyama, S., Takegawa, N., Kondo, Y., Schneider, J., Drewnick, F., Borrmann, S., Weimer, S., Demerjian, K., Williams, P., Bower, K., Bahreini, R., Cottrell, L., Griffin, R.J., Rautiainen, J., Sun, J.Y., Zhang, Y.M., Worsnop, D.R., 2007a. Ubiquity and dominance of oxygenated species in organic aerosols in anthropogenically-influenced Northern Hemisphere midlatitudes. Geophysical Research Letters 34, L13801.

Zhang, Q., Jimenez, J.L., Canagaratna, M.R., Ulbrich, I.M., Ng, N.L., Worsnop, D.R., Sun, Y., 2011. Understanding atmospheric organic aerosols via factor analysis of aerosol mass spectrometry: a review. Analytical and Bioanalytical Chemistry 401, 3045-3067.

Zhang, Q., Jimenez, J.L., Worsnop, D.R., Canagaratna, M., 2007b. A case study of urban particle acidity and its influence on secondary organic aerosol. Environmental Science & Technology 41, 3213-3219.

Zhao, P.S., Dong, F., Yang, Y.D., He, D., Zhao, X.J., Zhang, W.Z., Yao, Q., Liu, H.Y., 2013. Characteristics of carbonaceous aerosol in the region of Beijing, Tianjin, and Hebei, China. Atmospheric Environment 71, 389-398.

Zhong, C., Yang, Z.F., Jiang, W., Yu, T., Hou, Q.Y., Li, D.S., Wang, J.W., 2014. Annual input fluxes and source identification of trace elements in atmospheric deposition in Shanxi Basin: the largest coal base in China. Environmental Science and Pollution Research 21, 12305-12315.

Zhuang, B.L., Wang, T.J., Liu, J., Li, S., Xie, M., Yang, X.Q., Fu, C.B., Sun, J.N., Yin, C.Q., Liao, J.B., Zhu, J.L., Zhang, Y., 2014. Continuous measurement of black carbon aerosol in urban Nanjing of Yangtze River Delta, China. Atmospheric Environment 89, 415-424.

570 **Figure Captions:**

571 **Fig. 1.** Map of the sampling site, Xinzhou (the green flag).

572 **Fig. 2.** Time series of (a) wind speed (WS) color coded by wind direction (WD) and
573 pressure (*P*), (b) temperature (*T*) and precipitation (Precip.), (c) the mass
574 concentrations of PM_1 and black carbon (BC), and (d) sulfate, nitrate, ammonium,
575 organic aerosol and chloride.

576 **Fig. 3.** (a) Time series and (b) mass spectra profiles of three OA factors, i.e., HOA,
577 SV-OOA and LV-OOA. Also shown in (a) is the time series of external tracer species
578 including BC, ammonium, and sulfate.

579 **Fig. 4.** Average chemical composition of PM_1 and OA composition during (a) entire
580 study, and the periods with (b) low (< 35 $\mu g/m^3$, 54% of data points) and (c) high (≥
581 35 $\mu g/m^3$, 46% of data points) aerosol mass loadings.

582 **Fig. 5.** Average diurnal cycles of (a) WD and WS; (b) RH, *T*, and *P*; (c) NR-PM_1
583 species (organic aerosol, SO_4^{2-}, NO_3^-, NH_4^+, and Cl^-); (d) PM_1 ; (e) OA factors (HOA,
584 SV-OOA, LV-OOA) and BC; and (f) trace gases (NO_x, NO, O_3, and SO_2). The dash
585 lines show the mass fractions (right axis) of (c) aerosol species in PM_1, (e) BC in PM_1
586 and OA factors in total OA.

587 **Fig. 6.** Variations of (a) mass concentrations and (b) mass fractions of PM_1 species as
588 functions of WD, WS, RH and *T*.

589 **Fig. 7.** (a) The clustered 72-h backward trajectories at the height of 500 m for the
590 study period. The average composition of PM_1 associated with each cluster is shown
591 as the pie chart. The dash blue lines show all the backward trajectories for Cluster 2.
592 (b) Daily variations of PM_1 in Xinzhou and $PM_{2.5}$ in Beijing during this study period.

593

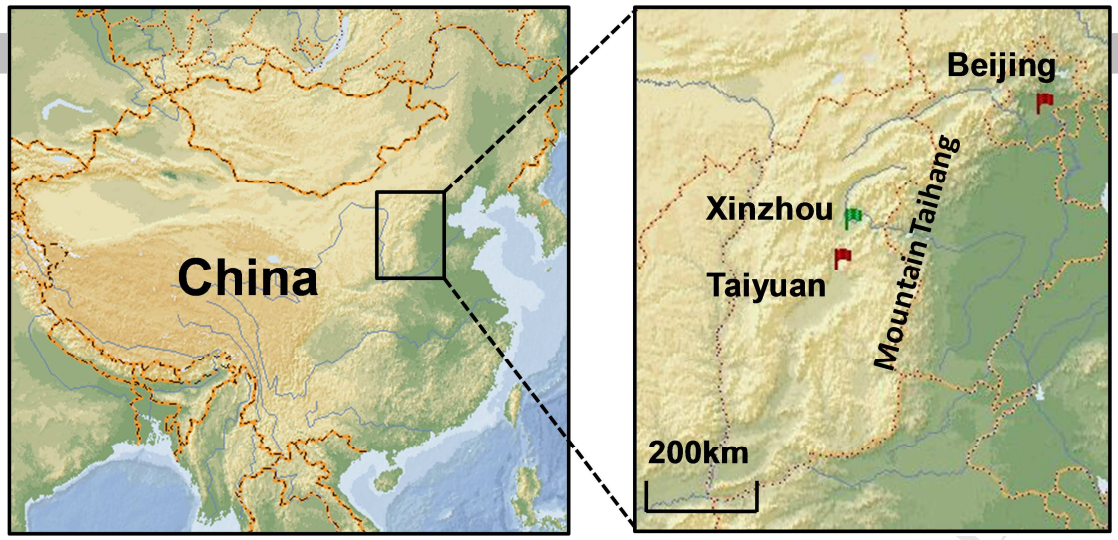

Fig. 1. Map of the sampling site, Xinzhou (the green flag).

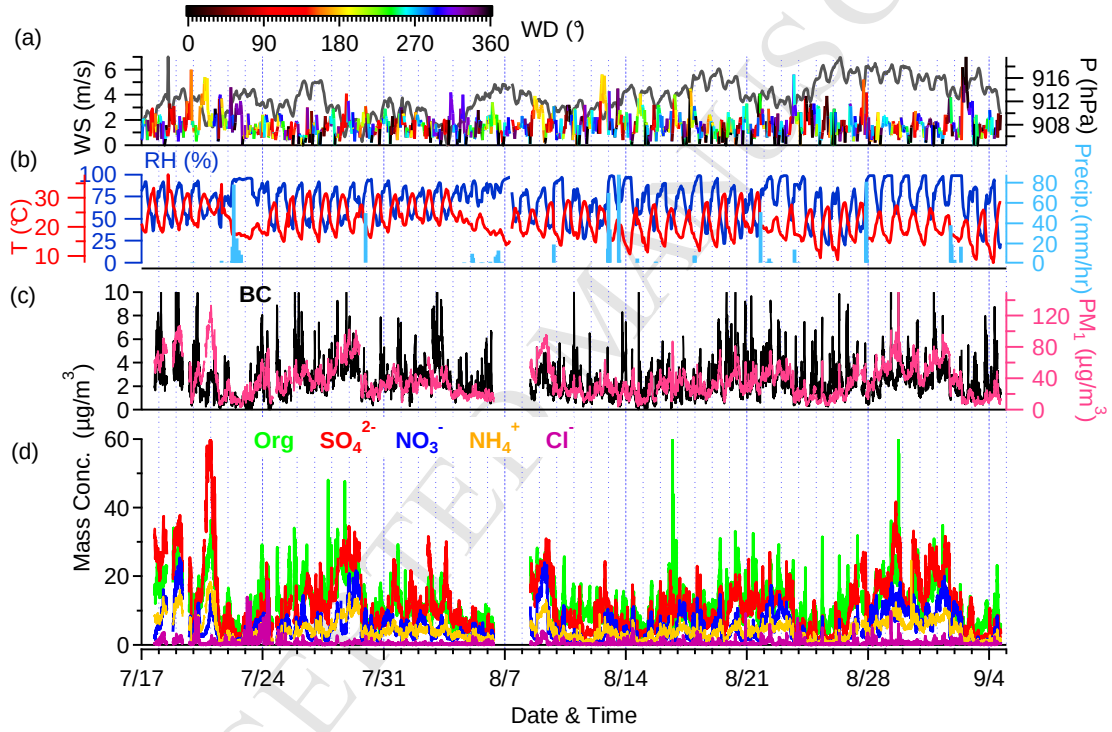

Fig. 2. Time series of (a) wind speed (WS) color coded by wind direction (WD) and pressure (*P*), (b) temperature (*T*) and precipitation (Precip.), (c) the mass concentrations of PM_1 and black carbon (BC), and (d) sulfate, nitrate, ammonium, organic aerosol and chloride.

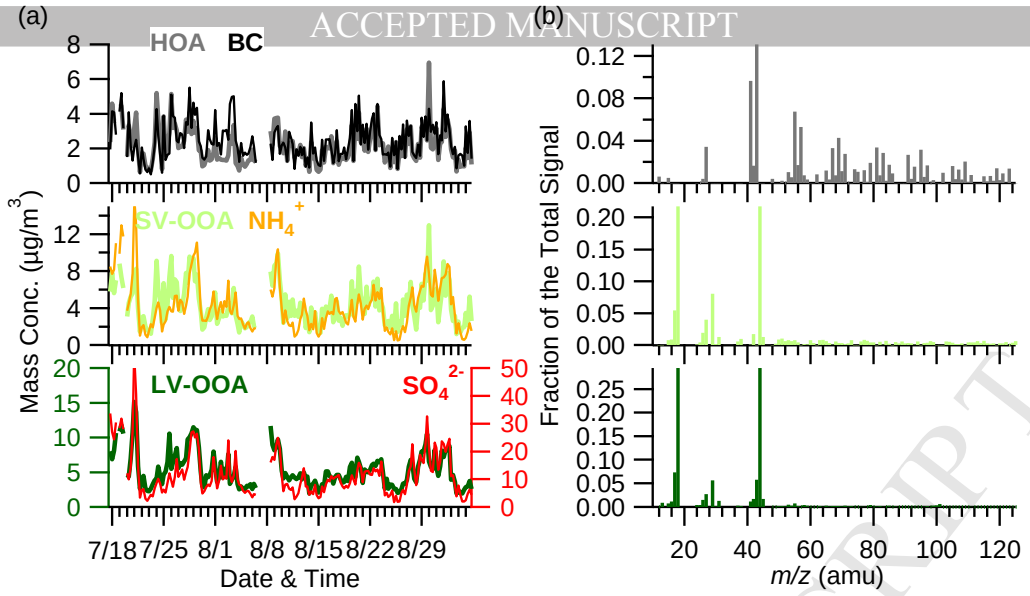

601

602 **Fig. 3.** (a) Time series and (b) mass spectra profiles of three OA factors, i.e., HOA,
603 SV-OOA and LV-OOA. Also shown in (a) is the time series of external tracer species
604 including BC, ammonium, and sulfate.

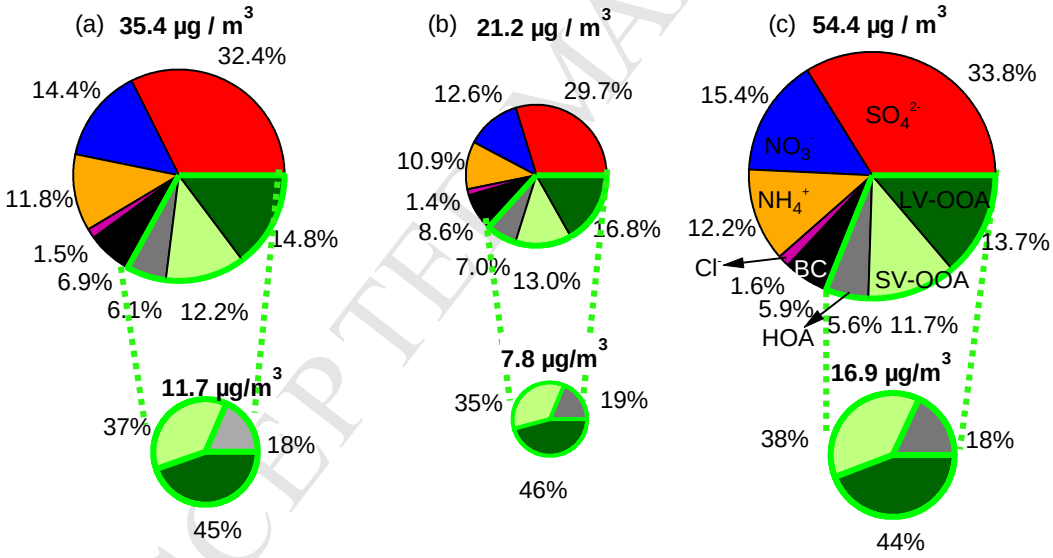

605

606 **Fig. 4.** Average chemical composition of PM_1 and OA composition during (a) entire
607 study, and the periods with (b) low (< 35 μg/m^3, 54% of data points) and (c) high (≥
608 35 μg/m^3, 46% of data points) aerosol mass loadings.

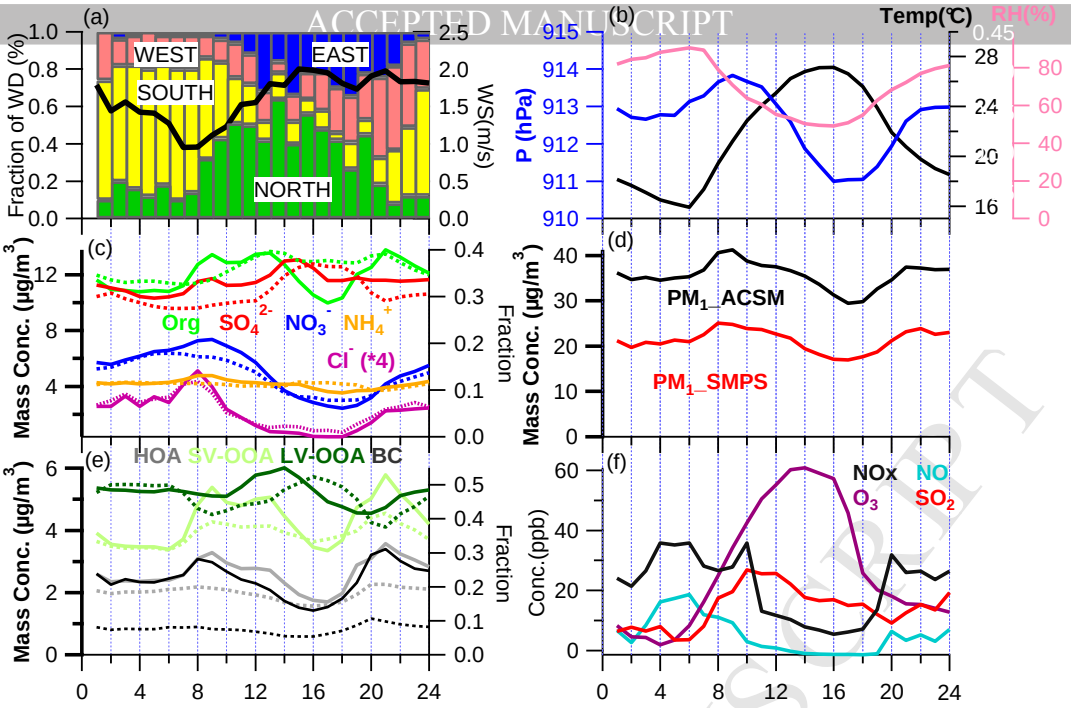

609

610 **Fig. 5.** Average diurnal cycles of (a) WD and WS; (b) RH, *T*, and *P*; (c) NR-PM_1
611 species (organic aerosol, SO_4^{2-}, NO_3^-, NH_4^+, and Cl^-); (d) PM_1 ; (e) OA factors (HOA,
612 SV-OOA, LV-OOA) and BC; and (f) trace gases (NO_x, NO, O_3, and SO_2). The dash
613 lines show the mass fractions (right axis) of (c) aerosol species in PM_1, (e) BC in PM_1
614 and OA factors in total OA.

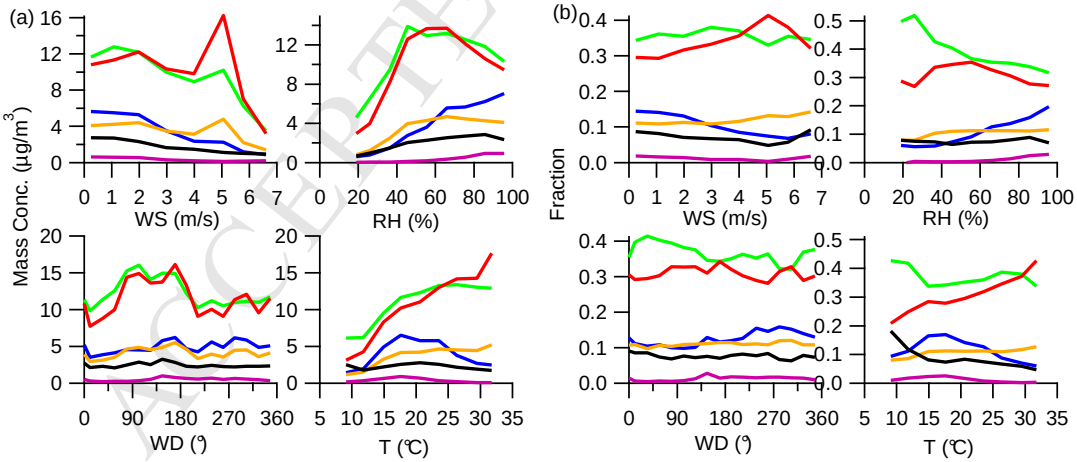

615

616 **Fig. 6.** Variations of (a) mass concentrations and (b) mass fractions of PM_1 species as
617 functions of WD, WS, RH and *T*.

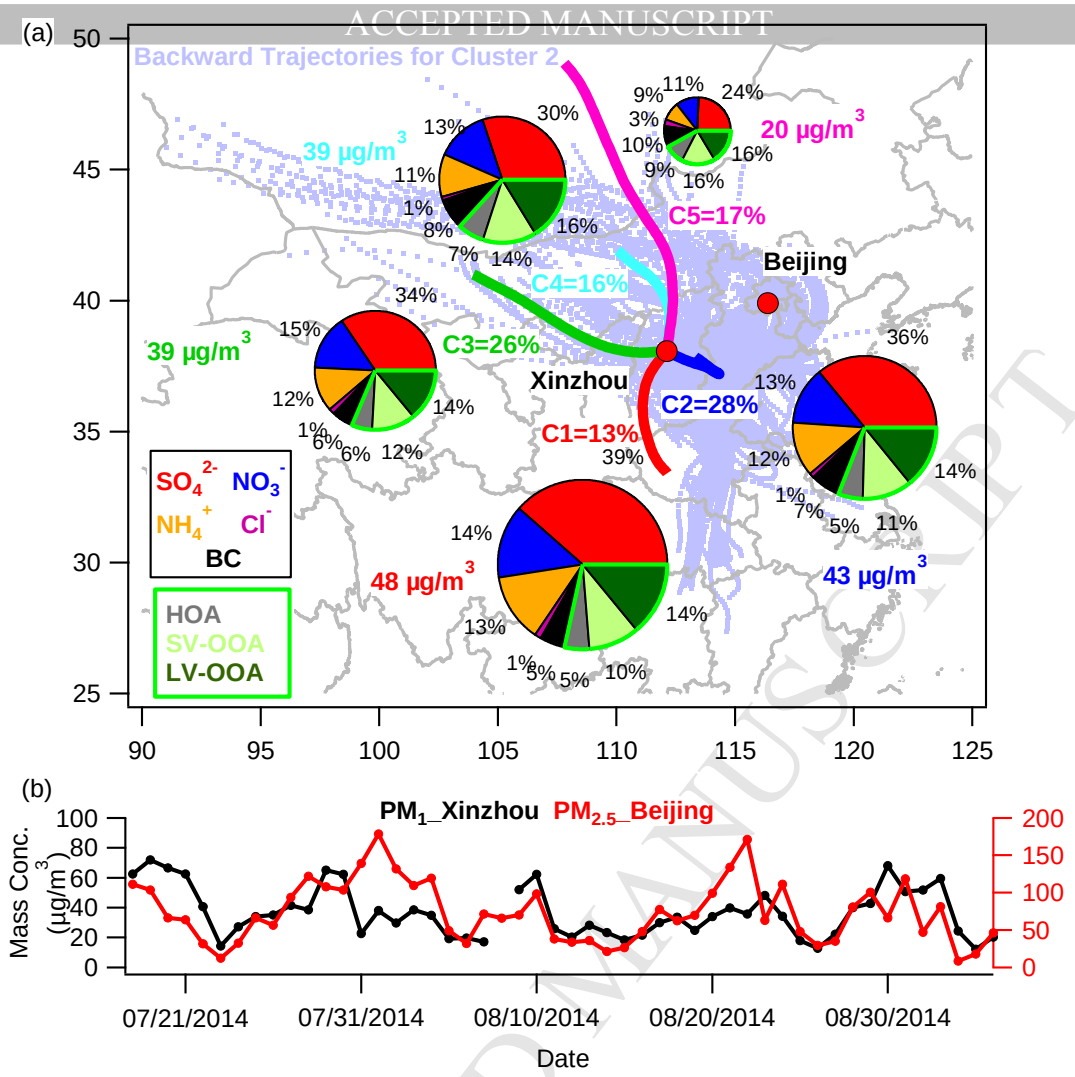

618

619 **Fig. 7.** (a) The clustered 72-h backward trajectories at the height of 500 m for the
620 study period. The average composition of PM_1 associated with each cluster is shown
621 as the pie chart. The dash blue lines show all the backward trajectories for Cluster 2.
622 (b) Daily variations of PM_1 in Xinzhou and $PM_{2.5}$ in Beijing during this study period.

- Submicron aerosol (PM_1) at a suburban site in Central China was characterized
- Organics and sulfate dominated PM_1 composition in central China
- Aerosol composition was relatively similar from different sources areas near the suburban site